
Semantic segmentation of sparse irregular point clouds for leaf/wood discrimination

Yuchen Bai¹ Jean-Baptiste Durand^{2*} Florence Forbes¹ Grégoire Vincent²

¹Univ. Grenoble Alpes, Inria, CNRS, Grenoble INP, LJK, Inria Grenoble Rhone-Alpes, France

²AMAP, Univ Montpellier, CIRAD, CNRS, INRAE, IRD, Montpellier, France

{yuchen.bai, florence.forbes}@inria.fr

jean-baptiste.durand@cirad.fr

gregoire.vincent@ird.fr

Abstract

LiDAR (Light Detection and Ranging) has become an essential part of the remote sensing toolbox used for biosphere monitoring. In particular, LiDAR provides the opportunity to map forest leaf area with unprecedented accuracy, while leaf area has remained an important source of uncertainty affecting models of gas exchanges between the vegetation and the atmosphere. Unmanned Aerial Vehicles (UAV) are easy to mobilize and therefore allow frequent revisits to track the response of vegetation to climate change. However, miniature sensors embarked on UAVs usually provide point clouds of limited density, which are further affected by a strong decrease in density from top to bottom of the canopy due to progressively stronger occlusion. In such a context, discriminating leaf points from wood points presents a significant challenge due in particular to strong class imbalance and spatially irregular sampling intensity. Here we introduce a neural network model based on the Pointnet ++ architecture which makes use of point geometry only (excluding any spectral information). To cope with local data sparsity, we propose an innovative sampling scheme which strives to preserve local important geometric information. We also propose a loss function adapted to the severe class imbalance. We show that our model outperforms state-of-the-art alternatives on UAV point clouds. We discuss future possible improvements, particularly regarding much denser point clouds acquired from below the canopy.

1 Introduction

In the past decade, LiDAR technology has been frequently used to acquire massive 3D data in the field of forest inventory (Vincent et al. [1]; Ullrich & Pfennigbauer [2]). The acquisition of point cloud data by employing LiDAR technology is referred to as laser scanning. The collected point cloud data provides rich details on tree structures, allowing us to calculate a key variable, leaf area, which controls water efflux and carbon influx. Monitoring leaf area should help in better understanding processes underlying flux seasonality in tropical forests, and is expected to enhance the precision of climate models for predicting the effects of global warming. There are various types of vehicles for data collection, with ground-based equipment and aircraft being the most commonly employed. The former operates a bottom-up scanning called terrestrial laser scanning (TLS), providing highly detailed and accurate 3D data. Scans are often acquired in a grid pattern every 10 m and co-registered into a single point cloud. However, TLS requires in-place intervention within the forest, which is laborious and limits its extensive implementation. Conversely, airborne laser scanning (ALS), which is much faster, can cover much larger areas. However, the achieved point density is typically two orders of magnitude smaller due to the combined effect of high flight altitude and fast movement

of the sensor. In addition, the occlusion caused by the upper tree canopy, makes it more difficult to observe the understory vegetation.

In recent years, the development of drone technology and the decreasing cost have led to UAV laser scanning (ULS) becoming one favoured option (Brede et al. [3]). It does not require in-situ intervention and each flight can be programmed to cover a few hectares. The acquired data is much denser than ALS (see Figure 1(a) and Figure 1(b)), which provide us with more comprehensive spatial information. Increasing the flight line overlap results in multiple angular sampling, higher point density and mitigates occlusions. Although the data density is still relatively low, compared with TLS, ULS can provide previously unseen overstory details due to the top-down view and overlap flight line. Furthermore, ULS is considered to be more suitable for conducting long-term monitoring of forests than TLS, as it allows pre-defined flight plans with minimal operator involvement.

Consequently, leaf-wood semantic segmentation in ULS data is a pressing demand, which is important for various applications, such as forest inventory, carbon sequestration, forest disease monitoring and harvest planning. Fulfilling these requirements necessitates the development of a robust algorithm that is capable to classify leaf and wood in forest environments. While numerous methods have demonstrated effective results on TLS data (see Section 2), these methods cannot be applied directly to ULS due to the class imbalance issue: leaf points account for about 95% of the data. Another problem is that many methods rely on the extra information provided by LiDAR devices, such as intensity. In the context of forest monitoring, intensity is not reliable due to frequent pulse fragmentation and variability in natural surface reflectivity (see Vincent et al. [5]). Furthermore, the reflectivity of the vegetation is itself affected by diurnal or seasonal changes in physical conditions, such as water content or orientation (Brede et al. [3]). Therefore, methods relying on intensity information (Wu et al. [6]) may exhibit substantial variations in performance across different locations and even within the same location but different acquisition batches. To address this issue, certain methods (LeWos proposed by Wang et al. [4]; Morel et al. [7]) have good results by exclusively utilizing the spatial coordinates of LiDAR data.

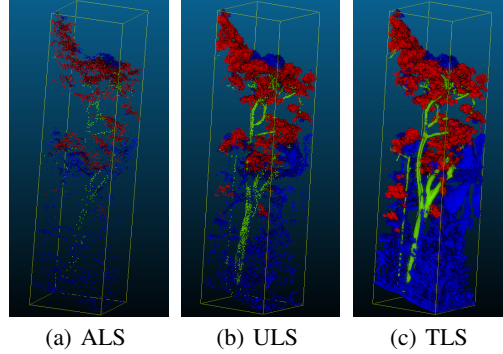


Figure 1: The captured points under three scanning modes on the same area ($20\text{m} \times 20\text{m} \times 42\text{m}$), illustrate how much the visibility of the understory differs. The colours in the figure correspond to different labels assigned to the points, where red and green indicate leaves and wood, respectively. Blue points are unprocessed, so labelled as unknown. The TLS data were initially subjected to semantic segmentation using LeWos [4] and subsequently manually corrected. Next, we use the K-nearest neighbours (KNN) algorithm to assign labels to ALS and ULS data based on the majority label among their five nearest neighbours in the TLS data.

Inspired by the existing methods, we propose a novel end-to-end approach **SOUL** (Semantic segmentation On ULs) based on PointNet++ proposed by Qi et al. [8] to perform semantic segmentation on ULS data. SOUL uses only point coordinates as the input, aiming to be applicable to forest data from various locations worldwide. The foremost concern to be tackled is the acquisition of labelled ULS data. Since no such dataset existed up to now, we gathered a ULS dataset comprising 282 trees labelled as shown in Figure 4. This was achieved through semi-automatic segmentation of a coincident TLS point cloud and wood/leaf label transfer to ULS point cloud. Secondly, the complex nature of tropical forests necessitates the adoption of a data pre-partitioning scheme. While certain methods (Krisanski et al. [9]; Wu et al. [10]) employ coarse voxels with overlap, such an approach leads to a fragmented representation and incomplete preservation of the underlying geometric information. The heterogeneous distribution of points within each voxel, including points from different trees and clusters at voxel boundaries, poses difficulties for data standardization. We introduce a novel data preprocessing methodology named geodesic voxelization decomposition (GVD), which leverages geodesic distance as a metric for partitioning the forest data into components and uses the topological features, like intrinsic-extrinsic ratio (IER) (He et al. [11]; Liu et al. [12]), to preserve the underlying geometric features at component level, see Section 3.2. The last issue concerns the class imbalance

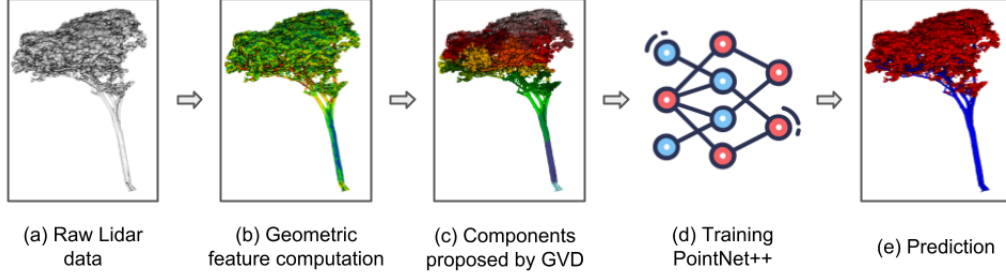


Figure 2: Overflow of SOUL. (a) We use only the coordinates of raw LiDAR data as input. (b) Geometric features like linearity, sphericity, verticality, and PCA1 are calculated at multiple scales using covariance and eigenvalues, then standardized. (c) GVD proposes components and performs data normalization within them. (d) Training deep neural network. (e) Finally, we obtain point-wise predictions while preserving the coordinates of raw data.

problem during the training stage. To address this issue, we developed a novel loss function named rebalanced loss, which yielded improved performance compared with the focal loss (Lin et al. [13]) for our specific task. This enhancement resulted in a 23% increase in the ability to recognize wood points, see Table 1.

The contribution of our work is three-fold. First, SOUL is the first approach developed to tackle the challenge of semantic segmentation on tropical forest ULS point clouds. SOUL demonstrates better wood point classification in complex tropical forest environments by exclusively utilizing point coordinates as input. Experiments show that SOUL exhibits promising generalization capabilities, achieving good performance even on datasets from other LiDAR devices, with a particular emphasis on overstory. Secondly, we propose a novel data preprocessing method, GVD, used to pre-partition data and address the difficult challenge of training neural network from sparse point clouds in tropical forest environments. Third, we mitigate the issue of imbalanced class by proposing a new loss function, referred to as rebalanced loss function, which is easy to use and can work as a plug-and-play for various deep learning architectures.

2 Related Works

Classical methods Classical methods are prevalent for processing point cloud data in forest environments, especially for semantic segmentation of TLS data, where they have achieved high levels of efficacy and applicability in practice. One such method, LeWos proposed by Wang et al. [4] uses geometric features and clustering algorithms, while an alternative method proposed by the first author of LeWos (Wang [14]) employs superpoint graphs (Landrieu & Simonovsky [15]). Moorthy et al. [16] use random forests (RF), and Zheng et al. [17] explore Gaussian mixture models. Other approaches, such as those proposed by Lalonde et al. [18], Itakura et al. [19], Vicari et al. [20], and Wan et al. [21], have also demonstrated successful semantic segmentation of TLS data.

Deep Learning methods Pioneering works like FSCT proposed by Krisanski et al. [9] and the method proposed by Morel et al. [7] have shown promising results by using PointNet++ [8]. Shen et al. [22] uses PointCNN (Li et al. [23]) as the backbone model to solve the problem of segmenting tree point clouds in artificially planted trees. Wu et al. [6] propose FWCNN, which incorporates intensity information and provides three new geometric features. Windrim & Bryson [10] propose a method that combines Faster R-CNN [24] and PointNet [25], which utilizes the bird’s eye view technique for single tree extraction and performs semantic segmentation on individual trees. In general, deep neural network-based approaches have demonstrated better performance in semantic segmentation of TLS point clouds compared with classical methods.

3 SOUL: Semantic segmentation on ULS

SOUL is based on PointNet++ Multi-Scale Grouping (MSG) [8] with some adaptations. The selection of PointNet++ is not only because of its demonstrated performance in similar tasks (Krisanski et al. [9]; Morel et al. [7]; Windrim & Bryson[10]), but also because of the lower GPU requirements (Choe et al. [26]) compared with transformer-based models developed in recent years, like the method proposed by Zhao et al. [27]. The main idea of SOUL lies in leveraging a geometric approach to extract preliminary features from the raw point cloud. These features are then combined with normalized coordinate into a deep neural network to obtain more abstract features from high dimensional space [25]. We will introduce our method in detail as follows.

3.1 Geometric feature computation

At this stage, we introduce four point-wise features: linearity, sphericity, verticality, and PCA1, which are computed at multiple scales of 0.3 m, 0.6 cm, and 0.9 cm in this task. To calculate these features, we need to construct the covariance matrix Σ for each point p_i , compute the corresponding eigenvalues $\lambda_1 > \lambda_2 > \lambda_3 > 0$ and the corresponding eigenvectors $e_1 e_2 e_3$. The local neighbours \mathcal{N}_{p_i} of p_i are given by:

$$\mathcal{N}_{p_i} = \{q \mid q \in \mathcal{P}, d_{ed}(p_i, q) \leq r\} \quad (1)$$

where \mathcal{P} is the component of all points and $r \in \{0.3, 0.6, 0.9\}$.

The covariance matrix Σ_{p_i} is:

$$\Sigma_{p_i} = \frac{1}{|\mathcal{N}_{p_i}|} \sum_{p_j \in \mathcal{N}_{p_i}} (p_j - \bar{p})(p_j - \bar{p})^T \quad (2)$$

where \bar{p} is the barycentre of \mathcal{N}_{p_i} .

The equations for computing the four characteristics are as follows:

Linearity 3 L_{p_i} serves as an indicator for the presence of a linear 1D structure (Weinmann et al. [28]).

$$L_{p_i} = \frac{\lambda_1 - \lambda_2}{\lambda_3} \quad (3)$$

Sphericity 4 S_{p_i} provide information regarding the presence of volumetric 3D structure (Weinmann et al. [28]).

$$S_{p_i} = \frac{\lambda_3}{\lambda_1} \quad (4)$$

Verticality 5 V_{p_i} indicate the property of being perpendicular to the horizon (Hackel et al. [29]), LeWos [4] uses it as a crucial feature because of its high sensitivity to the tree trunk. Here [001] is the vector of canonical basis.

$$V_{p_i} = 1 - |\langle [001], e_3 \rangle| \quad (5)$$

PCA1 6 $PCA1_{p_i}$ reflects the slenderness of \mathcal{N}_{p_i} . The direction of the first eigenvector e_1 is basically the most elongated in \mathcal{N}_{p_i} .

$$PCA1_{p_i} = \frac{\lambda_1}{\lambda_1 + \lambda_2 + \lambda_3} \quad (6)$$

Each point is endowed now with 12 features at 3 scales, enabling a precise depiction of its representation within the local structure. These features are subsequently standardized and integrated into the model's input as an extension to the point coordinates for the deep learning model.

3.2 Data pre-partitioning

The GVD algorithm 3.2 is used to partition the object into simpler geometric parts, which extract a set of representative training samples from raw forest data while preserving the local spatial geometry information in its entirety. The point cloud data is first voxelized into a voxel grid \mathcal{V} with a voxel

Algorithm 1 GVD

Input: Voxel grid \mathcal{V} ; gd threshold τ ; ier threshold γ **Output:** Components \mathbf{C}

```
1: function GVD( $\mathcal{V}$ ,  $\tau$ ,  $\gamma$ )
2:   while  $\mathcal{V} \neq \{\}$  do
3:      $i \leftarrow 0$  ▷ Component id
4:     Chose  $\hat{v} \in \mathcal{V}$ 
5:     while  $ier \leq \gamma$  and  $gd \leq \tau$  do
6:       Chose  $\bar{v} \in \mathcal{C}(\hat{v})$  ▷  $\mathcal{C}(\hat{v})$  arises from BFS on  $\hat{v}$ 
7:        $gd \leftarrow d_{gv}(\hat{v}, \bar{v})$ 
8:        $ier \leftarrow IER(\hat{v}, \bar{v})$  ▷ Eq. (8)
9:        $\mathbf{C} \leftarrow \mathbf{C} \cup \{i : \bar{v}\}$ 
10:    end while
11:     $i \leftarrow i + 1$ 
12:  end while
13:  Return  $\mathbf{C}$ 
14: end function
```

size s equal to 0.6 m, an empirical value. Each voxel v_i is considered as occupied if it contains at least one point. The geodesic-voxelization distance between any two voxels is defined as 1 if they are adjacent, and as the Manhattan distance between v_i and v_j in voxel space otherwise. This can be expressed mathematically as:

$$d_{gv}(v_i, v_j) = \begin{cases} 1, & \text{if } v_i \text{ and } v_j \text{ are adjacent} \\ |x_i - x_j| + |y_i - y_j| + |z_i - z_j|, & \text{otherwise} \end{cases} \quad (7)$$

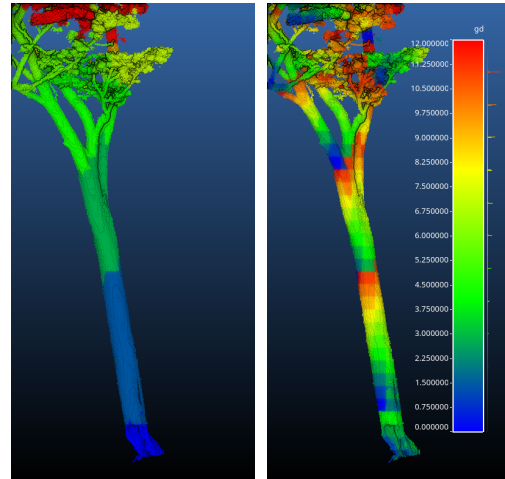
where (x_i, y_i, z_i) and (x_j, y_j, z_j) denote the coordinates of v_i and v_j respectively. We can establish an inter-voxel connectivity information with d_{gv} that enables the computation of the intrinsic-extrinsic ratio (IER):

$$IER(v_i, v_j) = \frac{d_{gv}(v_i, v_j)}{d_{ed}(v_i, v_j)} \quad (8)$$

where d_{ed} is the Euclidean distance. We find that d_{gv} and IER may provide strong cues for the subsequent segmentation task.

Subsequently, we chose one lowest voxel $\hat{v} \in \mathcal{V}$ on z-axis then employ the Breadth-first search (BFS) algorithm to explore its neighbours and the neighbours of neighbours $\mathcal{C}(\hat{v})$ and calculate corresponding $d_{gv}(\hat{v}, \bar{v})$ and $IER(\hat{v}, \bar{v})$ where $\bar{v} \in \mathcal{C}(\hat{v})$. This procedure terminates when the geodesic-voxelization distance d_{gv} exceeds τ or the IER exceeds γ . τ is set to 10 and γ is set to 1.5 in this task. All the points within $\mathcal{C}(\hat{v})$ are extracted from U and consolidated as a component \mathbf{C}_i of the point clouds (see Figure 3(a)). The whole procedure will be repeated until all the data is processed.

As the data is partitioned into multiple components, the points within one component \mathbf{C}_i are further sorted based on their geodesic-voxelization distance. In this arrangement, points inside one voxel v_i have the same geodesic distance $d_{gv}(\hat{v}, v_i)$, where \hat{v} is the lowest voxel inside \mathbf{C}_i (see Figure 3(b)). Thus, the GVD algorithm concludes at this stage.



(a) Trunk partitioned (b) Geodesic distance

Figure 3: (a) displays the components partitioned by the GVD, while (b) displays the geodesic distance within the corresponding component.

3.3 Normalization inside component

Shifting and scaling the point cloud coordinates before training a deep neural network is a widely adopted practice that can lead to improved training stability, generalization, and optimization efficiency, as Qi et al. [25] did. Here, prior to training the model, the point coordinates will be shifted to (0,0,0) and normalized by the longest axis among the three, all the point coordinates being confined within the (0,1) range. This prevents certain coordinates from dominating the learning process simply because they have larger values.

3.4 Training deep neural network

We employ a modified version of PointNet++ MSG for SOUL ([8]). The data combination of points and features within a component will be further partitioned into batches of 3000, which serve as the input for the network. If a batch within a component has fewer than 3000 points, the remaining points will be randomly chosen from the same component. The labels of the leaves and wood points correspond to 0 and 1, respectively. Define B_k as such a batch, $|B_k| = 3000$ and $B_k = B_{k,0} + B_{k,1}$ where $B_{k,0}$ and $B_{k,1}$ respectively represent the disjoint sub batch in B_k with ground-truth of leaf point and wood point.

Addressing class imbalance issue. Within the labelled ULS training dataset, only 4.4% are wood points, so the model is overwhelmed by the predominant features of leaves. Therefore, we propose a rebalanced loss L_R that changes the ratio of data participating to 1:1 at the loss calculation stage by randomly selecting a number of leaf points equal to the number of wood points.

In practice, the rebalanced loss is:

$$L_R(Y_{B_k}) = - \sum y_k \log(\hat{p}_k), \quad y_k \in (B'_{k,0} \cup B_{k,1}). \quad (9)$$

where Y_{B_k} specifies the ground truth label of the batch B_k , $\hat{p} \in [0, 1]$ is the model's estimated probability for the label $y = 1$ and $B'_{k,0}$ is defined as

$$B'_{k,0} = \begin{cases} \text{downsampling}(B_{k,0}, |B_{k,1}|), & \text{if } |B_{k,0}| \geq |B_{k,1}| \\ B_{k,0}, & \text{otherwise.} \end{cases} \quad (10)$$

where downsampling involves randomly selecting a subset of $B_{k,0}$ without replacement, with each point independently selected according to a uniform distribution. The size of the subset equals to $|B_{k,1}|$.

4 Experiments

We first provide more details about various LiDAR data present in each dataset. Second, we elaborate on the data preprocessing procedure. Next, we delve into the specific configurations of model hyperparameters during the training process, along with the adaptations made to the PointNet++ architecture. Following that, we showcase the performance of SOUL on the labelled ULS dataset. Finally, we demonstrate the generalization ability of SOUL on the other dataset.

Data details.

4.1 Data

The ULS data for this study were collected at the Research Station in French Guiana (N5°18' W52°53'). The Paracou forests are tropical forests situated in the lowlands of the Guiana Shield, the average height of the canopy is 27.2 m with top heights up to 44.8 m (Brede et al. [3]). We use four flights of ULS data on the same site in different time, the labelled data cover approximately 8000 m² of land. To facilitate model training and quantitative analysis, the labelled ULS data consisting of approximately 3.5 million points with a density of around 450 pts/m²¹ was partitioned into training,

¹Points per square meter.

validation, and test sets using a ratio of 6:2:2. In comparison, the point density of the labelled TLS data from the same site is about 320,000 pts/m².

In addition, we use two public datasets without labels only for exploring the model’s generalization ability. One is a ULS dataset from Sandhausen, Germany (Weiser et al. [30]), the other one is a mobile laser scanning (MLS)² dataset from New South Wales (NSW), Australia (NSW & Gonzalez S [31]). The Sandhausen dataset uses the same equipment as us but exhibits a lower point density of about 160 pts/m². The point density of NSW dataset is approximately 53,000 pts/m².

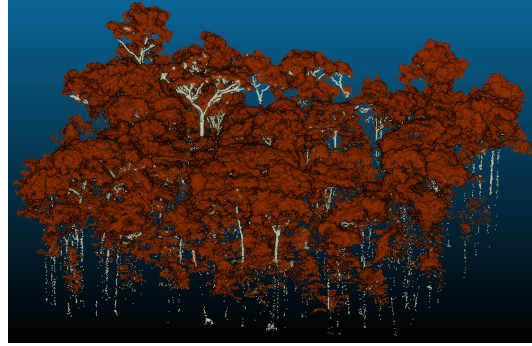


Figure 4: The labelled ULS dataset in French Guiana, where only 4.4% of the points correspond to wood. This significant class imbalance of leaf & wood presents a considerable challenge in discriminating wood points from forest point cloud.

4.1.1 Data preprocessing

The first step of the routine involves the data cleaning for TLS and ULS. The points exhibiting an intensity lower than -20 dB and those displaying high deviations (Pfennigbauer & Ullrich [32]) are removed, subsequently the TLS data are subsampled by setting a 0.001 m coordinate precision. The next stage is to separate ground by applying a cloth simulation filter (CSF) filter proposed by Zhang et al. [33], which mimics the physical phenomenon of a virtual cloth draped over an inverted point cloud. The ULS data will be subjected to a similar preprocessing pipeline, except that CSF on DLS (or ALS) performs poorly and was not used. Here we used TerraSolid ground detection algorithm on ALS and used the common ground model for all point clouds on the same place.

A subset of TLS trees with big trunk is labelled in using LeWos algorithm [4], followed by a manual refinement process to improve the outcome accuracy. Then the k-nearest neighbours algorithm (KNN) is employed to assign the label of TLS points to ULS points. Specifically, for each point in ULS dataset, the KNN algorithm selects five nearest points in the TLS dataset as reference points and subsequently determines the corresponding label based on the majority consensus of the reference points. It is noteworthy that within TLS data, there exist three distinct label types: unknown, leaf, and wood demonstrated in Figure 1(c), which respectively correspond to labels: -1, 0, and 1. The unknown label is also transferred to ULS points, then such points are filtered out for the next step. Unlabelled and therefore excluded points represent 65% of the ULS point cloud.

Implementation details. The Adam is chosen as the optimizer and the learning rate is 1e-7. Following the practice proposed by Smith et al. [34], we employ a strategy of gradually increasing the batch size by a factor of two approximately every 1000 epochs until reaching a final batch size of 128 instead of decreasing the learning rate during the training process. According to our experience, a favourable result needs a substantial duration, typically exceeding 3,000 epochs. In this paper, the prediction results are obtained from a checkpoint saved at the 3161st epoch. At this epoch, SOUL achieves a Matthews Correlation Coefficient (MCC)³ value of 0.605 (see Yao & Shepperd [35]) and an AUROC value of 0.888 on the validation dataset.

In our task, an output in the form of probability is preferred, as it is more consistent with the data collection process. However, to facilitate performance comparison with other methods, the model generates a discrete outcome that assigns a label to each point. The idea is if the probability of a point being classified as a leaf exceeds being as wood, it is labelled as a leaf and vice versa. Additionally, the probabilistic outputs indicating the likelihood of being a leaf or wood will be retained.

Results on French Guiana ULS data. Through a comparative analysis with the prevailing methods employed for forest point cloud, our approach SOUL improves semantic segmentation on ULS forest data by large margins. The results are summarized in Table 1, while Figure 5 highlight the performance

²The LiDAR device is integrated into a backpack, enabling a similar scanning process akin to TLS.

³MCC is a very good metric for evaluating binary classifier against class imbalance issue.

within the tree canopies. In terms of quantitative analysis, SOUL demonstrates a metric specificity of 63% in effectively discerning sparse wooden points, this value can be elevated to 79% but at the cost of decreasing the metric accuracy to 80% which is the metric for distinguishing leaf points. For better understanding how each class contributes to the overall performance, we introduced two more informative metrics mentioned in the study of Branco et al. [36], geometric mean (G-mean) and binary accuracy (BA). These metrics validate the performance of the SOUL model, providing more comprehensive insights into its capabilities.

Table 1: Comparison of different methods

Methods	Accuracy	Recall	Precision	Specificity	G-mean	BA ¹
FSCT [9]	0.974	0.977	0.997	0.13	0.356	0.554
FSCT + retrain	0.977	1.0	0.977	0.01	0.1	0.505
LeWos [4]	0.947	0.97	0.975	0.069	0.259	0.520
LeWos (SoD ²) [21]	0.953	0.977	0.975	0.069	0.260	0.523
SOUL (focal loss [13])	0.942	0.958	0.982	0.395	0.615	0.677
SOUL (rebalanced loss)	0.826	0.884	0.99	0.631	0.744	0.757

¹ BA (Balanced Accuracy) $BA = \frac{1}{2}(Recall + Specificity)$.

² SoD (Significant of Difference).

Results on the other data. After testing on datasets from Sandhausen dataset (Weiser et al. [30]) and NSW Forest dataset [31], we observed that the SOUL exhibits good generalization capability across various forests. Quantitative results demonstrated are shown in Figure 6. First, SOUL demonstrates good results on Sandhausen dataset [30]. However, SOUL doesn’t outperform the others methods on TLS, but it shows better discrimination within the tree canopy. A possible improvement is foreseen for denser data.

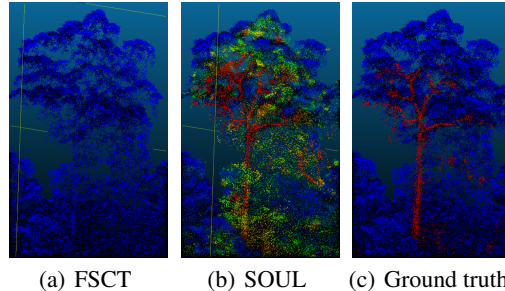


Figure 5: Qualitative results on ULS test dataset. Because of the class imbalance issue, methods such as FSCT[9], LeWos[4], and any other approaches developed for dense point cloud (cf. Section 2) are ineffective.

5 Discussion

Semantic segmentation in tropical forest environments presents distinctive challenges that differ from objects with regular shapes found in datasets such as ShapeNet (Chang et al. [37]) and ModelNet40 (Wu et al. [38]). Forest point clouds are inherently poorly structured and irregular because leaves and branches are small with regard to the lidar footprint size, a lot of points derived from LiDAR device are mixed by the two materials of leaves and wood. In addition, lots of points are a mix of both leaf and wood. So we propose GVD, an ad-hoc method for ULS data, to overcome the chaotic nature of forest point cloud by a pre-partition step. Similar to the enhancement that RCNN (Girshick et al. [39]) brings to CNN (LeCun et al. [40]) on 2D mission, GVD serves as a region proposal method that provides improved training sample for deep learning network. Our neural network can benefit from more refined and informative data, leading to enhanced performance in the semantic segmentation task.

In our methodology, PointNet++ is chosen as the backbone network due to its known robustness and effectiveness in extracting features from point clouds (Qian et al. [41]). But learning from imbalanced data in point cloud segmentation poses a persistent challenge, as discussed by Guo et al. [42]. To address this issue, we employ a rebalanced loss function tailored to this task. Rather than adjusting class weights during training (Lin et al. [13]; Sudre et al. [43]), we adopt a random selection approach to balance the training data during the loss computation. This decision stems from the observation that misprediction of a subset of the minority class can lead to significant fluctuations in the loss value, consequently inducing drastic changes in gradients. In an extreme scenario, wherein a single point represents a positive sample, correct prediction of this point drives the loss towards zero, irrespective of other point predictions. Conversely, misprediction of the single point yields a loss value approaching one.

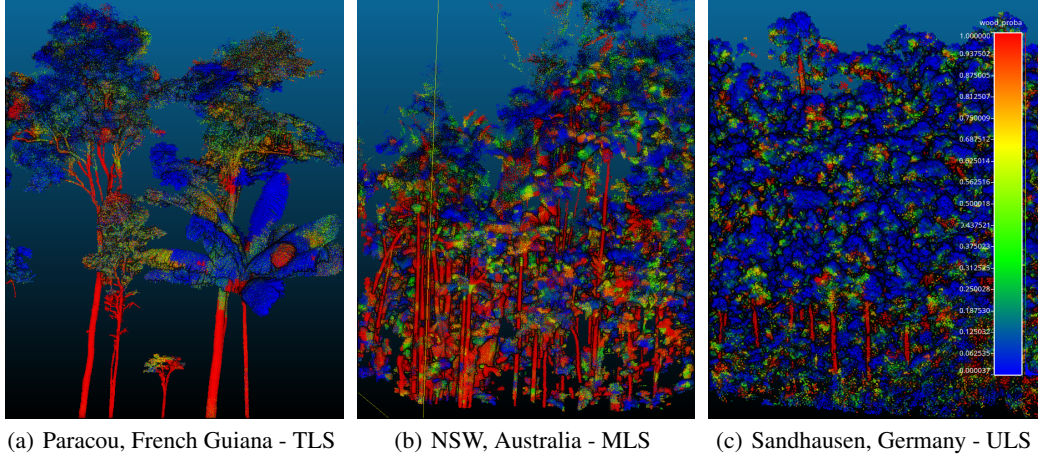


Figure 6: Qualitative results on various LiDAR data from different sites.

Despite being originally developed for tropical forest environments, SOUL demonstrates promising performance when applied to less complex forests. We anticipate that with the increasing prevalence of ULS data, coupled with more high-quality labelled datasets, the performance of SOUL is poised to advance further. Additionally, there is potential for SOUL to be extended to other complicated lidar scenes. It is conceivable to envision the development of a universal framework based on SOUL that can effectively handle various types of forest lidar data, including ULS, TLS, MLS, and even for ALS.

The current observation is that SOUL may not perform as well as other methods on TLS data, as it was not trained for that. Additionally, SOUL may not perform effectively for trees that significantly deviate from the training data. By incorporating diverse samples during training, the model can mitigate the challenges associated with vegetation disparity.

6 Conclusion

We present SOUL, a novel method for semantic segmentation in complex forest environments. It outperforms existing methods in the semantic segmentation of ULS tropical forest point clouds. It demonstrates high performance metrics on labelled ULS data and generalization capability across various forest datasets. The proposed GVD method is introduced as a solution to overcome the challenge by providing refined training sample through pre-partition. One key aspect of SOUL is the use of rebalanced loss function, which prevents drastic changes in gradients and improving segmentation accuracy. While SOUL shows good performance for different forest types, it may struggle with significantly different trees without retraining. Future work can focus on improving the performance of SOUL on denser forest point cloud to broaden its applications.

References

- [1] G. Vincent, C. Antin, M. Laurans, J. Heurtebize, S. Durrieu, C. Lavalley, and J. Dauzat, "Mapping plant area index of tropical evergreen forest by airborne laser scanning. a cross-validation study using lai2200 optical sensor," *Remote Sensing of Environment*, vol. 198, pp. 254–266, 2017.
- [2] A. Ullrich and M. Pfennigbauer, "Categorisation of full waveform data provided by laser scanning devices," Oct 2011.
- [3] B. Brede, H. M. Bartholomeus, N. Barbier, F. Pimont, G. Vincent, and M. Herold, "Peering through the thicket: Effects of uav lidar scanner settings and flight planning on canopy volume discovery," *International Journal of Applied Earth Observation and Geoinformation*, vol. 114, p. 103056, 2022.

- [4] D. Wang, S. Momo Takoudjou, and E. Casella, “Lewos: A universal leaf-wood classification method to facilitate the 3d modelling of large tropical trees using terrestrial lidar,” *Methods in Ecology and Evolution*, vol. 11, no. 3, pp. 376–389, 2020.
- [5] G. Vincent, P. Verley, B. Brede, G. Delaitre, E. Maurent, J. Ball, I. Clocher, and N. Barbier, “Multi-sensor airborne lidar requires intercalibration for consistent estimation of light attenuation and plant area density,” *Remote Sensing of Environment*, vol. 286, p. 113442, 2023.
- [6] B. Wu, G. Zheng, and Y. Chen, “An improved convolution neural network-based model for classifying foliage and woody components from terrestrial laser scanning data,” *Remote Sensing*, vol. 12, no. 6, 2020.
- [7] J. Morel, A. Bac, and T. Kanai, “Segmentation of unbalanced and in-homogeneous point clouds and its application to 3d scanned trees,” Sep 2020.
- [8] C. R. Qi, L. Yi, H. Su, and L. J. Guibas, “Pointnet++: Deep hierarchical feature learning on point sets in a metric space,” *CoRR*, vol. abs/1706.02413, 2017.
- [9] S. Krisanski, M. S. Taskhiri, S. Gonzalez Aracil, D. Herries, A. Muneri, M. B. Gurung, J. Montgomery, and P. Turner, “Forest structural complexity tool—an open source, fully-automated tool for measuring forest point clouds,” *Remote Sensing*, vol. 13, no. 22, 2021.
- [10] L. Windrim and M. Bryson, “Detection, segmentation, and model fitting of individual tree stems from airborne laser scanning of forests using deep learning,” *Remote Sensing*, vol. 12, no. 9, 2020.
- [11] T. He, H. Huang, L. Yi, Y. Zhou, C. Wu, J. Wang, and S. Soatto, “Geonet: Deep geodesic networks for point cloud analysis,” 2019.
- [12] M. Liu, X. Zhang, and H. Su, “Meshing point clouds with predicted intrinsic-extrinsic ratio guidance,” 2020.
- [13] T.-Y. Lin, P. Goyal, R. Girshick, K. He, and P. Dollár, “Focal loss for dense object detection,” 2018.
- [14] D. Wang, “Unsupervised semantic and instance segmentation of forest point clouds,” *ISPRS Journal of Photogrammetry and Remote Sensing*, vol. 165, pp. 86–97, 2020.
- [15] L. Landrieu and M. Simonovsky, “Large-scale point cloud semantic segmentation with super-point graphs,” 2018.
- [16] S. M. Krishna Moorthy, K. Calders, M. B. Vicari, and H. Verbeeck, “Improved supervised learning-based approach for leaf and wood classification from lidar point clouds of forests,” *IEEE Transactions on Geoscience and Remote Sensing*, vol. 58, no. 5, pp. 3057–3070, 2020.
- [17] G. Zheng, L. Ma, W. He, J. U. H. Eitel, L. M. Moskal, and Z. Zhang, “Assessing the contribution of woody materials to forest angular gap fraction and effective leaf area index using terrestrial laser scanning data,” *IEEE Transactions on Geoscience and Remote Sensing*, vol. 54, no. 3, pp. 1475–1487, 2016.
- [18] J.-F. Lalonde, N. Vandapel, and M. Hebert, “Automatic three-dimensional point cloud processing for forest inventory,” Tech. Rep. CMU-RI-TR-06-21, Carnegie Mellon University, Pittsburgh, PA, July 2006.
- [19] K. Itakura, S. Miyatani, and F. Hosoi, “Estimating tree structural parameters via automatic tree segmentation from lidar point cloud data,” *IEEE Journal of Selected Topics in Applied Earth Observations and Remote Sensing*, vol. 15, pp. 555–564, 2022.
- [20] M. B. Vicari, M. Disney, P. Wilkes, A. Burt, K. Calders, and W. Woodgate, “Leaf and wood classification framework for terrestrial lidar point clouds,” *Methods in Ecology and Evolution*, vol. 10, no. 5, pp. 680–694, 2019.
- [21] P. Wan, J. Shao, S. Jin, T. Wang, S. Yang, G. Yan, and W. Zhang, “A novel and efficient method for wood-leaf separation from terrestrial laser scanning point clouds at the forest plot level,” *Methods in Ecology and Evolution*, vol. 12, no. 12, pp. 2473–2486, 2021.

- [22] X. Shen, Q. Huang, X. Wang, J. Li, and B. Xi, "A deep learning-based method for extracting standing wood feature parameters from terrestrial laser scanning point clouds of artificially planted forest," *Remote Sensing*, vol. 14, no. 15, 2022.
- [23] Y. Li, R. Bu, M. Sun, W. Wu, X. Di, and B. Chen, "Pointcnn: Convolution on \mathcal{X} -transformed points," 2018.
- [24] S. Ren, K. He, R. Girshick, and J. Sun, "Faster r-cnn: Towards real-time object detection with region proposal networks," 2016.
- [25] C. R. Qi, H. Su, K. Mo, and L. J. Guibas, "Pointnet: Deep learning on point sets for 3d classification and segmentation," 2017.
- [26] J. Choe, C. Park, F. Rameau, J. Park, and I. S. Kweon, "Pointmixer: Mlp-mixer for point cloud understanding," 2022.
- [27] H. Zhao, L. Jiang, J. Jia, P. Torr, and V. Koltun, "Point transformer," 2021.
- [28] M. Weinmann, B. Jutzi, and C. Mallet, "Feature relevance assessment for the semantic interpretation of 3d point cloud data," *ISPRS Annals of the Photogrammetry, Remote Sensing and Spatial Information Sciences*, vol. II-5/W2, pp. 313–318, 2013.
- [29] T. Hackel, J. D. Wegner, and K. Schindler, "Contour detection in unstructured 3d point clouds," in *2016 IEEE Conference on Computer Vision and Pattern Recognition (CVPR)*, pp. 1610–1618, 2016.
- [30] H. Weiser, L. Winiwarter, V. Zahs, P. Weiser, K. Anders, and B. Höfle, "UAV-Photogrammetry, UAV laser scanning and terrestrial laser scanning point clouds of the inland dune in Sandhausen, Baden-Württemberg, Germany," 2022.
- [31] N. R. C. N. Government and G. S, "Nsw forest monitoring and improvement program forest plot network ground based lidar pilot," 2022.
- [32] M. Pfennigbauer and A. Ullrich, "Improving quality of laser scanning data acquisition through calibrated amplitude and pulse deviation measurement," in *Laser Radar Technology and Applications XV* (M. D. Turner and G. W. Kamerman, eds.), vol. 7684 of *Society of Photo-Optical Instrumentation Engineers (SPIE) Conference Series*, p. 76841F, Apr. 2010.
- [33] W. Zhang, J. Qi, P. Wan, H. Wang, D. Xie, X. Wang, and G. Yan, "An easy-to-use airborne lidar data filtering method based on cloth simulation," *Remote Sensing*, vol. 8, no. 6, 2016.
- [34] S. L. Smith, P.-J. Kindermans, C. Ying, and Q. V. Le, "Don't decay the learning rate, increase the batch size," 2018.
- [35] J. Yao and M. Shepperd, "Assessing software defection prediction performance," in *Proceedings of the Evaluation and Assessment in Software Engineering*, ACM, apr 2020.
- [36] P. Branco, L. Torgo, and R. P. Ribeiro, "A survey of predictive modeling on imbalanced domains," *ACM Comput. Surv.*, vol. 49, aug 2016.
- [37] A. X. Chang, T. Funkhouser, L. Guibas, P. Hanrahan, Q. Huang, Z. Li, S. Savarese, M. Savva, S. Song, H. Su, J. Xiao, L. Yi, and F. Yu, "Shapenet: An information-rich 3d model repository," 2015.
- [38] Z. Wu, S. Song, A. Khosla, F. Yu, L. Zhang, X. Tang, and J. Xiao, "3d shapenets: A deep representation for volumetric shapes," 2015.
- [39] R. Girshick, J. Donahue, T. Darrell, and J. Malik, "Rich feature hierarchies for accurate object detection and semantic segmentation," 2014.
- [40] Y. LeCun, B. Boser, J. S. Denker, D. Henderson, R. E. Howard, W. Hubbard, and L. D. Jackel, "Backpropagation applied to handwritten zip code recognition," *Neural Comput.*, vol. 1, p. 541–551, dec 1989.

- [41] G. Qian, Y. Li, H. Peng, J. Mai, H. A. A. K. Hammoud, M. Elhoseiny, and B. Ghanem, "Pointnext: Revisiting pointnet++ with improved training and scaling strategies," 2022.
- [42] Y. Guo, H. Wang, Q. Hu, H. Liu, L. Liu, and M. Bennamoun, "Deep learning for 3d point clouds: A survey," 2020.
- [43] C. H. Sudre, W. Li, T. Vercauteren, S. Ourselin, and M. J. Cardoso, "Generalised dice overlap as a deep learning loss function for highly unbalanced segmentations," in *Deep Learning in Medical Image Analysis and Multimodal Learning for Clinical Decision Support*, pp. 240–248, Springer International Publishing, 2017.
- [44] J. Wojtanowski, M. Zygmunt, M. Kaszczuk, Z. Mierczyk, and M. Muzal, "Comparison of 905 nm and 1550 nm semiconductor laser rangefinders' performance deterioration due to adverse environmental conditions," *Opto-Electronics Review*, vol. 22, no. 3, pp. 183–190, 2014.
- [45] D. P. Kingma and J. Ba, "Adam: A method for stochastic optimization," 2017.
- [46] D.-A. Clevert, T. Unterthiner, and S. Hochreiter, "Fast and accurate deep network learning by exponential linear units (elus)," 2016.
- [47] V. Nair and G. E. Hinton, "Rectified linear units improve restricted boltzmann machines," in *Proceedings of the 27th International Conference on International Conference on Machine Learning*, ICML'10, (Madison, WI, USA), p. 807–814, Omnipress, 2010.
- [48] A. Paszke, S. Gross, F. Massa, A. Lerer, J. Bradbury, G. Chanan, T. Killeen, Z. Lin, N. Gimelshein, L. Antiga, A. Desmaison, A. Kopf, E. Yang, Z. DeVito, M. Raison, A. Tejani, S. Chilamkurthy, B. Steiner, L. Fang, J. Bai, and S. Chintala, "Pytorch: An imperative style, high-performance deep learning library," in *Advances in Neural Information Processing Systems* 32, pp. 8024–8035, Curran Associates, Inc., 2019.

Supplementary

A Overview

In this supplementary material, we provide more quantitative results, technical details and additional qualitative test examples. In section B, we first present more implementation and training details of SOUL and in section C we conduct ablation studies to investigate the impact of different loss functions on the model’s performance. At last, we demonstrate the performance improvement achieved by using multiple-scale computation of geometric features comparing to single-scale in section D. We have made a video showcasing the performance of SOUL, the link is provided here.

B Additional Implementation Details

LiDAR scanner. Table 2 presents a summary of the distinguishing laser characteristics between ULS and TLS. The acquisition of LiDAR data is profoundly impacted by atmospheric characteristics, the LiDAR extinction coefficients exhibit a low impact to atmospheric humidity at both 905 nm and 1550 nm wavelengths (Wojtanowski et al. [44]). ULS uses 905 nm as wavelength, at which the scanning device has the minimum energy consumption (Brede et al. [3]). Meanwhile, the TLS system operates at a wavelength of 1550 nm, which is more susceptible to the fog impact (Wojtanowski et al. [44]). This poses the issue that the spectral reflectance of vegetation is more varied (Brede et al. [3]) at the 905 nm wavelength, thereby leading us to employ only point coordinates as input for avoiding the use of intensity information.

Table 2: Laser sensor characteristics

	TLS	ULS
Riegl Scanner	VZ400	miniVux-1UAV
Laser Wavelength (nm)	1550	905
Beam divergence (mrad)	≤ 0.25	$\leq 1.6^{\circ}$
Footprint diameter (cm@100m)	3.5	16*5
Pulse duration (ns)	3	6
Range resolution (m)	0.45	0.9

Training details. In addition to the content already illustrated in the main paper, we provide further details regarding the training parameters. First and foremost, sufficient training time is required for the model to achieve desirable performance. Our observation indicates that models trained less than 2000 epochs are inadequately trained to achieve desirable performance. During the training process, three metrics, AUROC, MCC and Specificity, are considered more informative and insightful. Especially, the metric of specificity is crucial as it measures the ability to accurately discriminate wooden points, which is the primary requirement of our method. Another thing to note is that, contrary to the mentioned practice in the main text of increasing the batch size by a factor of two every 1000 epochs, we did not strictly follow this restriction during the actual training process. Often, the increase in batch size occurred around 800-900 or 1100-1200 epochs for better using the GPU resources. However, theoretically, this offset shouldn’t affect the final performance.

Architecture of DL model. We have made several modifications to the architecture of PointNet++ (MSG) [8]. Firstly, we observed that Adam (Kingma & Ba [45]) outperformed Nesterov SGD in this task, and ELU (Clevert et al. [46]) activation function is better than ReLU (Nair & Hinton [47]). The fraction of the input units to drop for dropout layer is changed from 0.5 to 0.3, that means the probability of an element to be zeroed is 30% (Paszke et al. [48]). We also decrease the output from 256 to 128 and add two more fully connected layers at the end.

Test with error bar. We have calculated a confidence interval at 95% confidence level to indicate the uncertainty of our method. In the main body of the paper, it was mentioned that we obtained data from four flights, and each data collection from these flights allowed us to obtain a labelled ULS dataset through label transfer from TLS data. The test dataset is composed by 40 trees from the

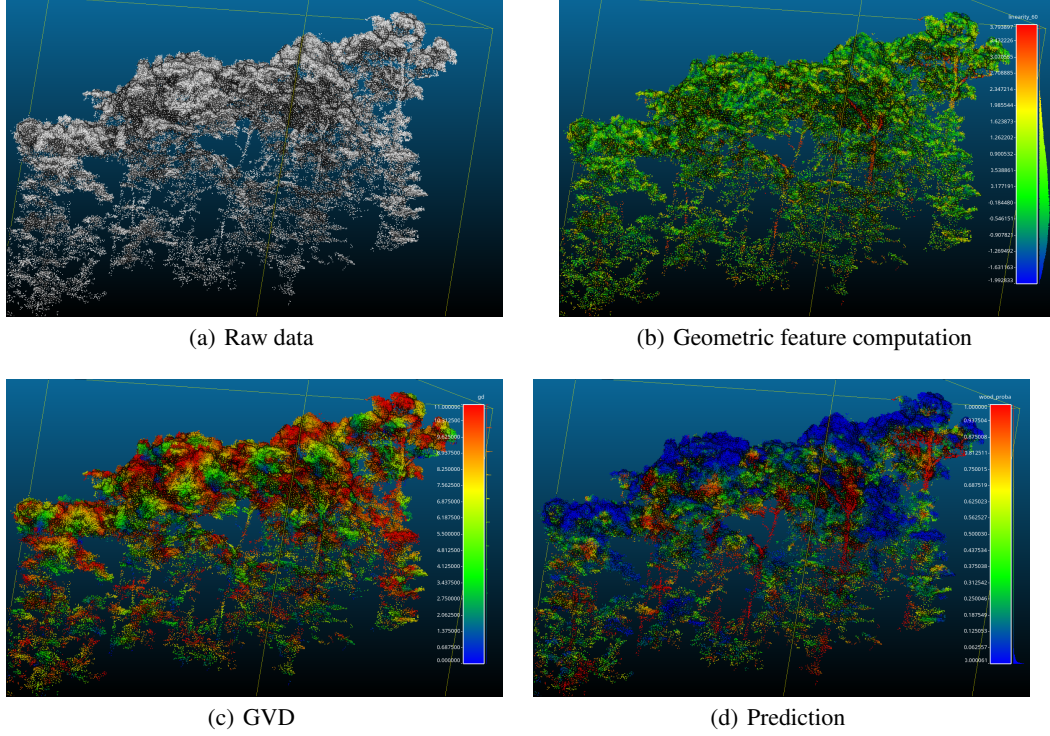


Figure 7: SOUL routine

same positions across these four labelled ULS datasets, resulting in a total of 160 trees. We divided further these 160 trees based on their unique tree IDs to 16 smaller test sets. However, trees with the same tree ID are not placed together in the same test set. The calculation of confidence intervals was derived from these 16 test sets. The result is summarized in Table 3 and Table 4. It is evident that SOUL outperforms all other methods on ULS data and achieves state-of-the-art performance on metrics such as Specificity, Balanced Accuracy and G-mean.

Table 3: Comparison of different methods

Methods	Specificity	G-mean	BA ¹
FSCT [9]	0.13	0.356	0.554
FSCT + retrain	0.01	0.1	0.505
LeWos [4]	0.069	0.259	0.520
LeWos (SoD ²) [21]	0.069	0.260	0.523
SOUL (focal loss [13])	0.395	0.615	0.677
SOUL (rebalanced loss)	0.576 ± 0.063	0.651 ± 0.030	0.720 ± 0.027

¹ BA (Balanced Accuracy) $BA = \frac{1}{2}(Recall + Specificity)$.

² SoD (Significant of Difference).

Output contains redundant points. To proceed with further data analysis and usage, it is necessary to remove duplicate points present in the output.

C Ablation study

In this section, we mainly discuss the significant benefits introduced by the rebalanced loss. The network is biased towards leaf points in using cross entropy loss function and the use of focal loss function (Lin et al. [13]) did not yield substantial improvements to the task, as its performance remained unsatisfactory when tested on the raw dataset (see Figure 8(a) and Figure 8(b)).

Table 4: Comparison of different methods

Methods	Accuracy	Recall	Precision
FSCT [9]	0.974	0.977	0.997
FSCT + retrain	0.977	1.0	0.977
LeWos [4]	0.947	0.97	0.975
LeWos (SoD) [21]	0.953	0.977	0.975
SOUL (focal loss [13])	0.942	0.958	0.982
SOUL (rebalanced loss)	0.857 ± 0.014	0.865 ± 0.015	0.988 ± 0.002

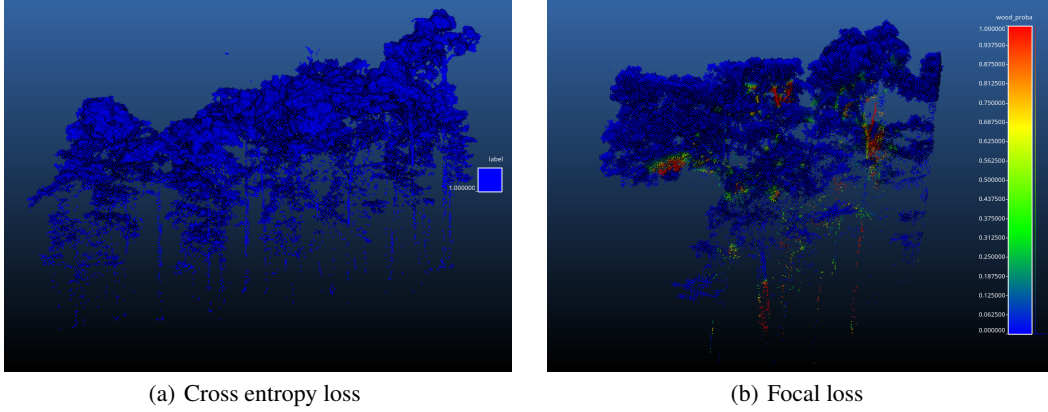


Figure 8: Cross entropy loss function and focal loss function on raw ULS data. Blue represents wood points with high probability, while red represents leaf points with high probability. Despite utilizing focal loss, the model remains overwhelmed by leaf points.

Through a comparison of the specificity curves (see focal loss specificity in Figure 9 versus rebalanced loss specificity in Figure 10) and the training/validation loss curves of focal loss and rebalanced loss (see loss curve of focal loss in Figure 11 versus loss curve of rebalanced loss in Figure 12), we observed that focal loss failed to address the issue of class imbalance in our task. Plus, it is important to note that in the loss curve of rebalanced loss, the validation loss curve showed significant fluctuations in Figure 12. As foreseen, this variation occurred because the training process employing the rebalanced loss for model training, while the validation process utilized the cross-entropy loss function. Consequently, the loss value used for backpropagation is derived from the rebalanced loss function, which inherently does not consider the majority of leaf points. So once using cross entropy to calculate the loss, all points within a batch are taken into account, which can lead to fluctuations in the validation loss curve. However, it was expected that the validation loss curve would eventually converge on the validation set to demonstrate that using rebalanced loss for backward propagation effectively balances the representation of leaf and wood points. In fact, the final results surpassed focal loss by a significant margin (see Figure 7), as evidenced by the convergence of the validation loss curve for rebalanced loss (see Figure 12). For the loss curve of focal loss in Figure 11, both the training and validation processes employ the focal loss function.

In Figure 10, Figure 12 and Figure 14, we can clearly observe the presence of "sharp drops", which are a result of the operation mentioned on main paper and Section B, where we increased the batch size by a factor of two approximately every 1000 epochs. We followed this practice proposed by Smith et al. [34], which involves increasing the batch size instead of decaying the learning rate.

D Single-scale vs Multiple-scale

In this section, we mainly showcase multiple-scale geometric features calculation outperform single-scale at our task. After applying the rebalanced loss as the loss function, we observed that computing geometric features at multiple scales ultimately improved the performance of SOUL. When comparing the evolution of specificity with the number of epochs between single-scale and multiple-scale (see

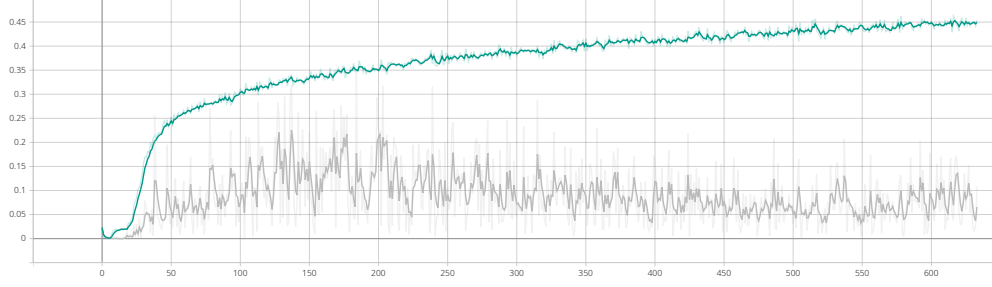


Figure 9: Specificity - focal loss (single-scale feature calculation). In the figure, the cyan curve represents the specificity curve of the training dataset, while the gray curve represents the specificity curve of the validation dataset.

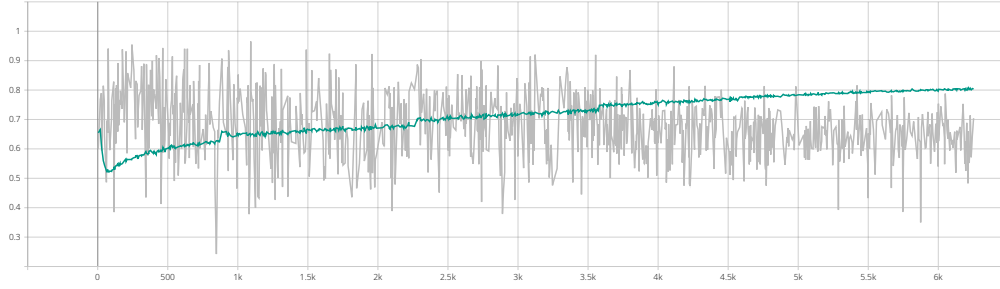


Figure 10: Specificity - rebalanced loss (single-scale feature calculation), cyan curve - training dataset, gray curve - validation dataset.

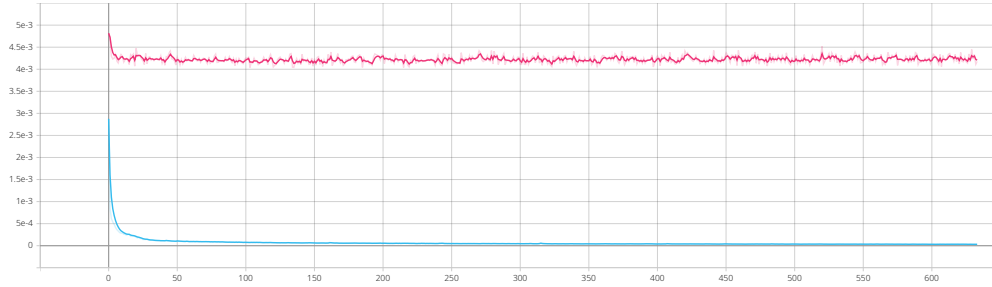


Figure 11: Loss - focal loss (single-scale feature calculation). The blue curve represents the loss curve of the training dataset, while the red curve represents the loss curve of the validation dataset.

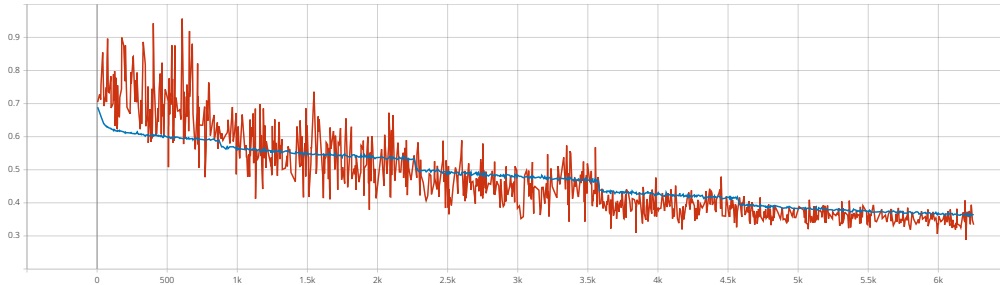


Figure 12: Loss - rebalanced loss (single-scale feature calculation), blue curve - training dataset, red curve - validation dataset.

Figure 13 and Figure 14), multiple-scales not only exhibit higher values but also converge more effectively over time.

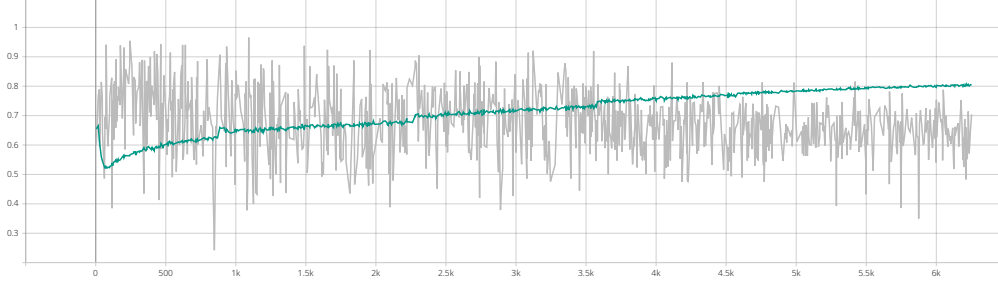


Figure 13: Specificity - Single-scale geometric features calculation, cyan curve - training dataset, gray curve - validation dataset.

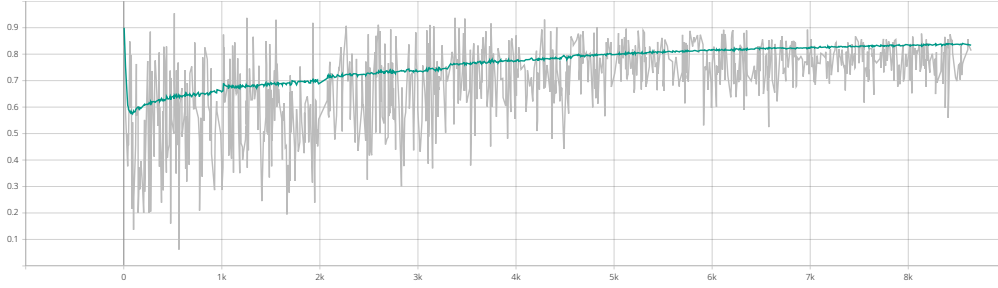


Figure 14: Specificity - Multiple-scale geometric features calculation, cyan curve - training dataset, gray curve - validation dataset.

The Matthews Correlation Coefficient (MCC) (see Yao & Shepperd [35]) and AUROC are both effective metrics to evaluate the model performance under class imbalance issue. Therefore, besides the specificity, we provide the MCC and AUROC values for both single-scale and multiple-scale cases during the training process. Upon analysing the comparative results of MCC in Figure 15 and Figure 16, and AUROC in Figure 17 and Figure 18, we consistently observe that the multiple-scale computation of geometric features output higher values compared to the single-scale. This strongly supports the superior performance of multiple-scale feature computation over single-scale.

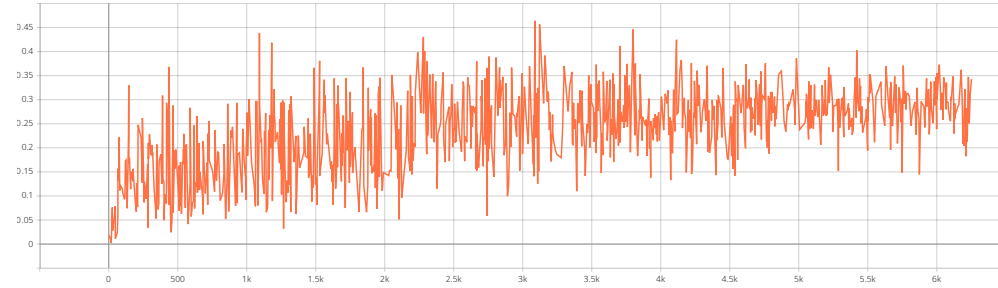


Figure 15: During the training process, the MCC (single-scale) values change with the number of epochs.

MCC and AUROC provide valuable insights for selecting the final model state (checkpoint). For example, up to now, the best-performing model state is the one obtained at the 3161st epoch with the multiple-scale geometric features computation, as mentioned in the main paper. The model achieves an MCC value of 0.605 and an AUROC value of 0.888, these results generally outperform all single-scale metrics. As MCC is a discrete case of Pearson correlation coefficient, we can conclude that there exists a strong positive relationship exists between the model's predictions and the ground truth by using the interpretation of Pearson correlation coefficient.

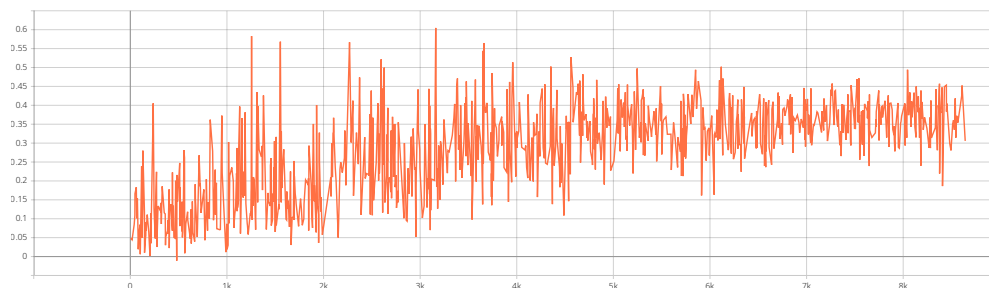


Figure 16: MCC (multiple-scale) values change with the number of epochs.

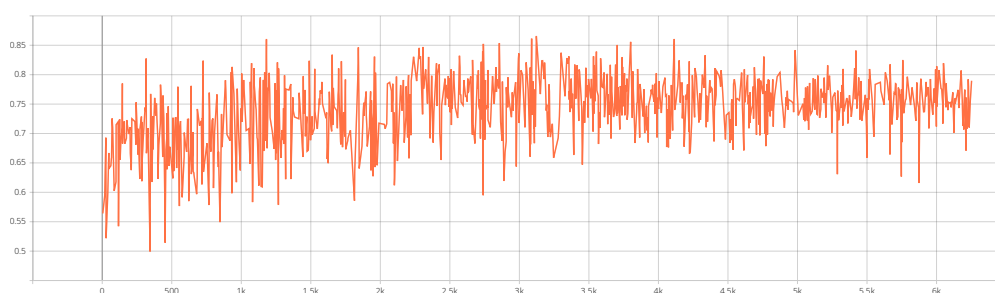


Figure 17: AUROC (single-scale) values change with the number of epochs.

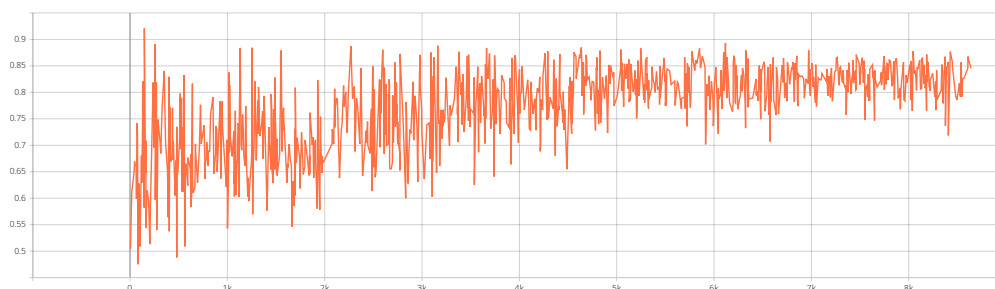


Figure 18: AUROC (single-scale) values change with the number of epochs.